Electronic Supplementary Information

Experimental Section

Materials: Sodium nitrite ($NaNO_2$, 99.0%), ammonium chloride (NH_4Cl, 99.99%), sodium hydroxide (NaOH, 99.9%), sodium salicylate ($C_7H_5NaO_3$，99.5%~100.3%), salicylic acid ($C_7H_6O_3$, 99.5%), trisodium citrate dihydrate ($C_6H_5Na_3O_7 \cdot 2H_2O$, 99.0%), p-dimethylaminobenzaldehyde ($C_9H_{11}NO$, 99.0%), sodium nitroferricyanide dihydrate ($C_5FeN_6Na_2O \cdot 2H_2O$, 99%), and sodium hypochlorite solution (NaClO, Available chlorine ≥5.5%) are purchased from Aladdin Ltd. (Shanghai, China). Nickel hexahydrate chloride ($NiCl_2 \cdot 6H_2O$, ≥98.0%), and ammonium chloride (NH_4Cl, 99.99%) were purchased from Chengdu Kelong Chemical Regent Co. Ltd. Sulfuric acid (H_2SO_4, 98.3%), hydrogen peroxide (H_2O_2, 30 wt% in H_2O), hydrochloric acid (HCl， 36.0~38.0%), hydrazine monohydrate ($N_2H_4 \cdot H_2O$, >98%) and ethanol (C_2H_5OH, 99.5%) were bought from Beijing Chemical Corporation. (China). chemical Ltd. in Chengdu. Carbon paper was purchased from Qingyuan Metal Materials Ni, Ltd (Xingtai, China). All reagents used in this work were analytical grade without further purification.

Preparation of pure JBC-800：The juncus was ultrasonically washed with distilled water and then dried at 60 °C for 24 h. The dried juncus was calcined at 800 °C for 2 h in Ar with a heating rate of 2 °C min^{-1}. Finally, the juncus cooled to room temperature was collected and the obtained product was named as JBC-800.

Preparation of Ni@JBC-700, Ni@JBC-800, and Ni@JBC-900: In brief, 0.15 g of juncus was immersed into the 30 mL 0.05 M $NiCl_2 \cdot 6H_2O$ solution for 12 h. The soaked juncus was then washed with distilled water and dried at 60 °C overnight. Subsequently, the pretreated samples were calcined at 700, 800, and 900 ℃ for 2 h under argon atmosphere, the resulting products were named Ni@JBC-700, Ni@JBC-800, and Ni@JBC-900, respectively.

Characterizations: XRD data were acquired by a LabX XRD-6100 X-ray diffractometer with a Cu Kα radiation (40 kV, 30 mA) of wavelength 0.154 nm

(SHIMADZU, Japan). SEM measurements were carried out on a GeminiSEM 300 scanning electron microscope (ZEISS, Germany) at an accelerating voltage of 5 kV. The absorbance data of spectrophotometer were measured on UV-Vis spectrophotometer. TEM image was obtained from a Zeiss Libra 200FE transmission electron microscope operated at 200 kV.

Electrochemical measurements: 10 mg catalyst and 40 μL 5 wt% Nafion were dispersed in 960 μL of water/ethanol solution (v/v = 1:3) by sonicating for 2 h to get a homogeneous catalyst ink. Then, a certain volume of the ink was dropped onto a 0.25 cm^2 carbon paper with a catalyst loading of 0.2 mg cm^{-2} and dried at room temperature. All electrochemical measurements were performed in a two-compartment cell separated by a treated Nafion 117 membrane using the CHI660E electrochemical workstation (Shanghai, Chenhua) with a standard three-electrode setup. Electrolyte solution was Ar-saturated 0.1 M NaOH with 0.1 M $NaNO_2$, using Ni@JBC-800 (0.2 mg cm^{-2}) as the working electrode, a graphite rod as the counter electrode and a Hg/HgO as the reference electrode. All the potentials reported in our work were converted to reversible hydrogen electrode (RHE) scale via calibration with the following equation: E (RHE) = E (vs. Hg/HgO) + 0.0591 × pH + 0.098 V and the current density was normalized by the geometric surface area.

Determination of NH_3: Concentration of produced NH_3 was determined by spectrophotometry measurement with indophenol blue method (the obtained electrolyte was diluted 20 times). In detail, 2 mL of the diluted catholyte was obtained from the cathodic chamber and mixed with 2 mL of 1.0 M NaOH solution containing salicylic acid and sodium citrate. Then, 1 mL of 0.05 M NaClO and 0.2 mL of 1 wt% $C_5FeN_6Na_2O$ were dropped in the collected electrolyte solution. After standing at room temperature for 2 h, the UV-Vis absorption spectrum was measured. The concentration-absorbance curve was calibrated using the standard NH_4Cl solution with NH_3 concentrations of 0, 0.2, 0.5, 1.0, 2.0, and 5.0 μg mL^{-1} in 0.1 M NaOH. The absorbance at 655 nm was measured to quantify the NH_3 concentration using standard NH_4Cl solutions ($y = 0.399\ x + 0.03488$, $R^2 = 0.9998$) (Fig. S5).

Determination of N_2H_4: In this work, we used the method of Watt and Chrisp to

determine the concentration of produced N_2H_4. The chromogenic reagent was a mixed solution of 5.99 g $C_9H_{11}NO$, 30 mL HCl, and 300 mL C_2H_5OH. In detail, 1 mL electrolyte was added into 1 mL prepared color reagent and stirred for 15 min in the dark. The absorbance at 455 nm was measured to quantify the N_2H_4 concentration with a standard curve of hydrazine ($y = 0.65285\ x + 0.06748$, $R^2 = 0.9992$) (Fig. S6).

Determination of gaseous products: Gaseous products from nitrate reduction reaction were determined by GC (SHIMADZU GC-2014 gas chromatograph). A GC run was initiated per 1200 s. Argon (99.999%) was used as the carrier gas. A flame ionization detector with a thermal conductivity detector (TCD) was used to quantify hydrogen and nitrogen. In our work, the H-type cell is hermetically sealed and tightly connected with the gas sampling loop of the GC. Before the test, Ar was poured into the H-type cell for 5 min to ensure that gases such as N_2 and O_2 in the electrolyzer were completely removed. During the test, the carrier gas flows into the electrolyzer with a constant flow rate of 30 sccm, and then enters the gas inlet of the GC after passing through the electrolyte. The carrier gas carried gaseous products was introduced into a condenser before being vented directly into the gas sampling loop of the GC.

Calculations of the FE and NH_3 yield:

Equations of cathode reaction of NO_2^-RR:

$$NO_2^- + 6e^- + 6H_2O \rightarrow NH_4^+ + 8OH^-, \text{ in alkaline media} \quad (1)$$

Equations of anode reaction:

$$4OH^- \rightarrow 2H_2O + O_2 + 4e^- \quad (2)$$

Possible overall reaction:

$$2NO_2^- + 6H_2O \rightarrow 3O_2 + 2NH_4^+ + 4OH^- \quad (3)$$

FE toward NH_3 via NO_2^-RR was calculated by equation:

$$FE = 6 \times F \times ([NH_4^+] \times V / M_{NH4^+}) / Q \times 100\% \quad (4)$$

NH_3 yield was calculated using the following equation:

$$NH_3 \text{ yield rate} = [NH_4^+] \times V / (M_{NH4^+} \times t \times m_{cat}) \quad (5)$$

Where F is the Faradic constant (96485 C mol^{-1}), $[NH_3]$ is the measured NH_3 concentration, V is the volume of electrolyte in the anode compartment (35 mL),

M_{NH4}^{+} is the molar mass of NH_4^+, Q is the total quantity of applied electricity; t is the electrolysis time and m_{cat} is the loaded mass of catalyst.

Computational details: First-principles calculations were performed by using the Vienna Ab initio Simulation Package (VASP)[1-4] to investigate the NO_2^-RR process on Ni@JBC-800 surface. The valence-core electrons interactions were treated by Projector Augmented Wave (PAW) potentials and the electron exchange correlation interactions were described by the generalized gradient approximation (GGA) with the Perdew-Burke-Ernzerhof (PBE) functional.[5,6] Considered long-range interaction at the interface, Van der Waals interactions were considered using DFT-D3 correlation.[7] To avoid interaction come from other slabs, a vacuum of 20 Å was added along z direction. The convergence criterion of geometry relaxation was set to 0.03 $eV \cdot Å^{-1}$ in force on each atom. The energy cutoff for plane wave-basis was set to 500 eV. The K points were sampled with 3 × 3 × 1 by Monkhorst-Pack method.[8]

Gibbs free energy change (ΔG) was evaluated based on the computational hydrogen electrode (CHE) model, which takes one-half of the chemical potential of gaseous hydrogen under standard conditions as the free energy of the proton-electron pairs. ΔG were calculated by the following equation:[9]

$$\Delta G = \Delta E + \Delta E_{ZPE} - T\Delta S + neU$$

where ΔE, ΔE_{ZPE}, ΔS are the reaction energy from DFT calculation, the correction of zero-point energy and the change of simulated entropy, respectively. T is the temperature (T = 300 K). n and U are the number of transferred electrons and applied potential, respectively.

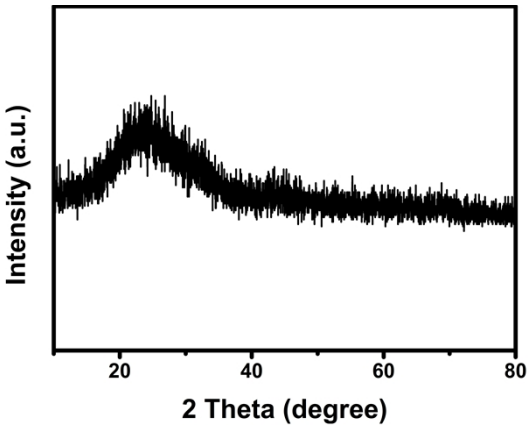

Fig. S1. XRD pattern of JBC-800.

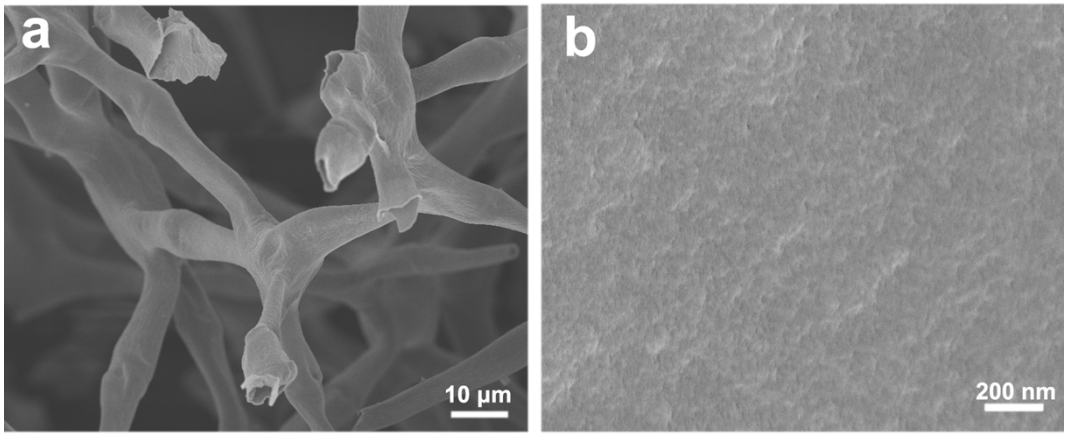

Fig. S2. SEM images of JBC-800.

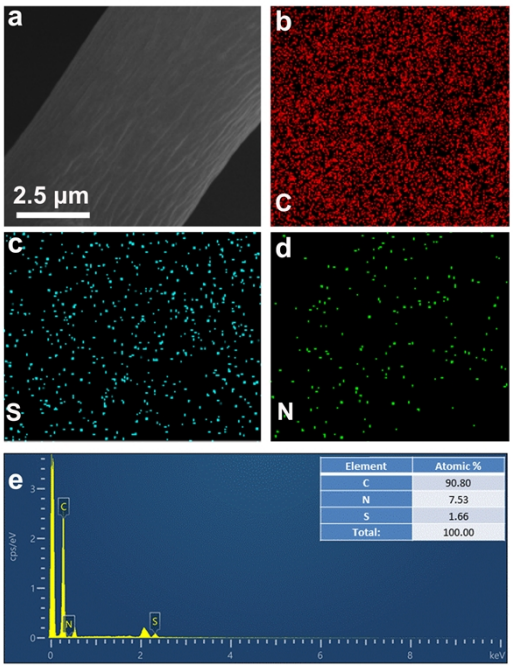

Fig. S3. (a-d) SEM and EDX elemental mapping images and (e) EDX spectrum of JBC-800.

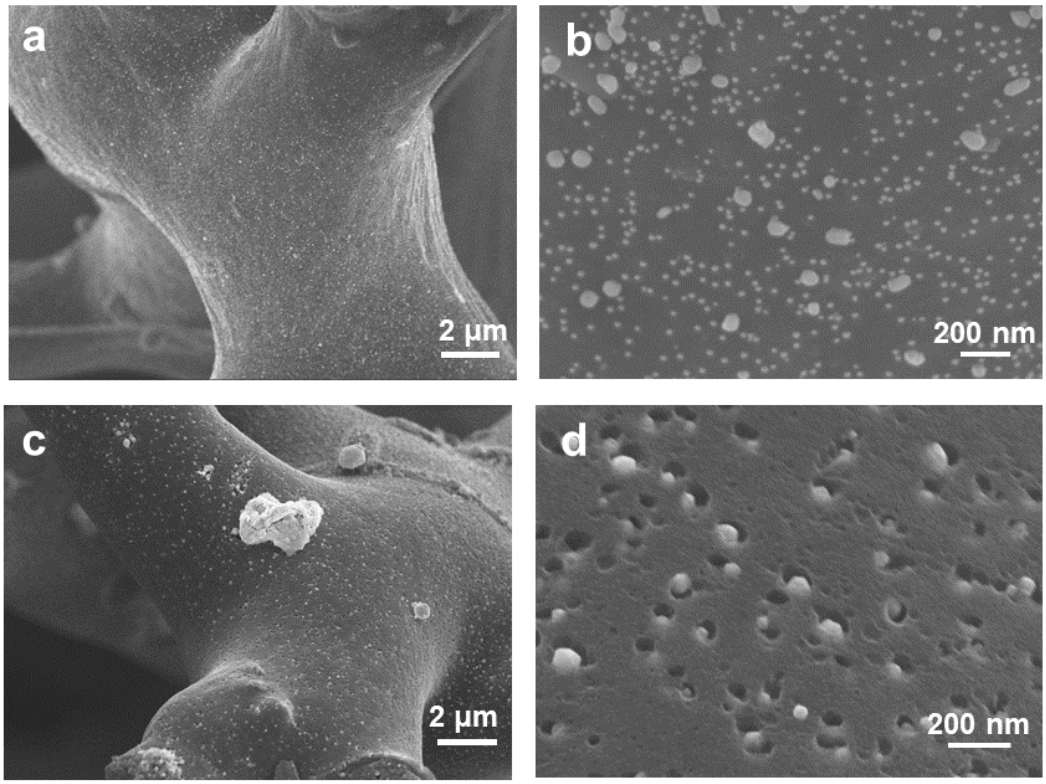

Fig. S4. SEM images of (a and b) Ni@JBC-700 and (c and d) Ni@JBC-900.

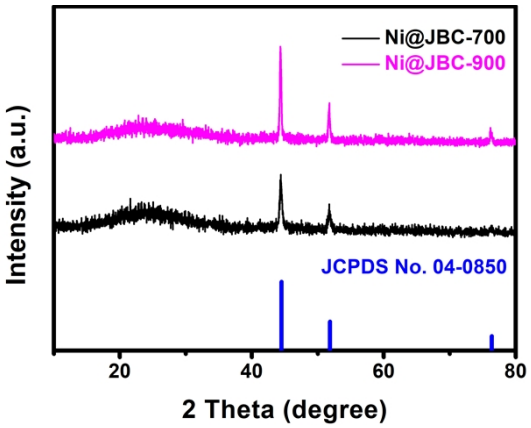

Fig. S5. XRD patterns of Ni@JBC-700 and Ni@JBC-900.

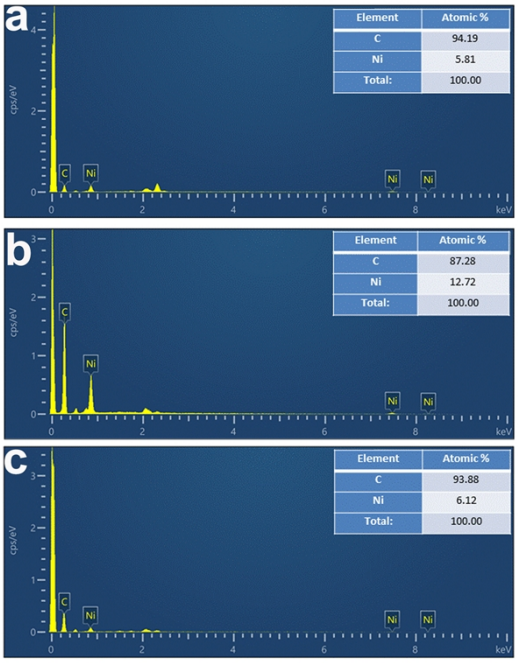

Fig. S6. EDX spectra of (a) Ni@JBC-700, (b) Ni@JBC-800, and (c) Ni@JBC-900.

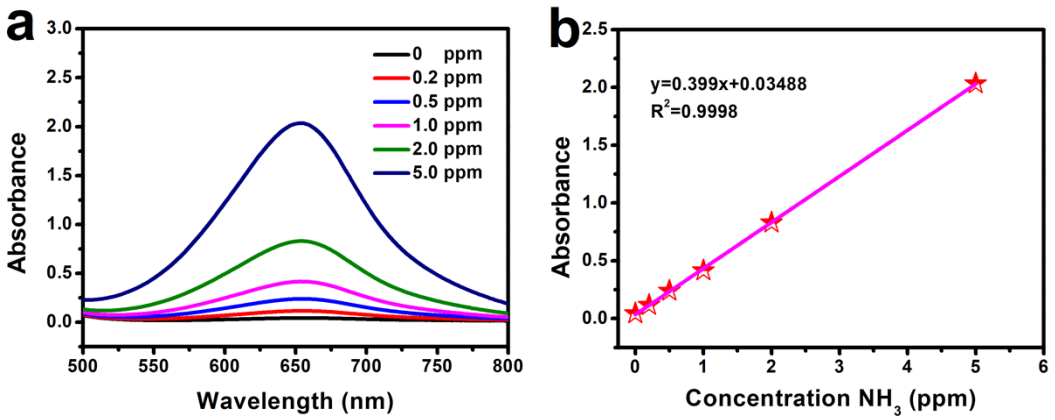

Fig. S7. (a) UV-Vis spectra and (b) corresponding calibration curve for determining NH_3.

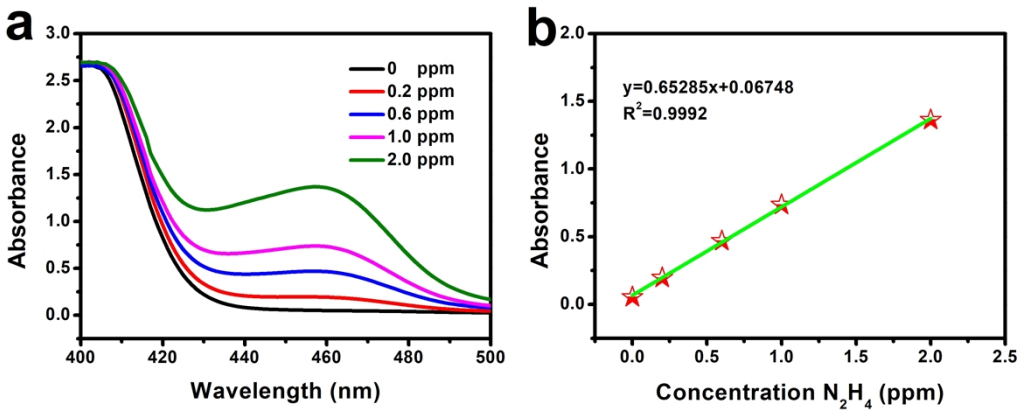

Fig. S8. (a) UV-Vis spectra and (b) corresponding calibration curve for determining N_2H_4.

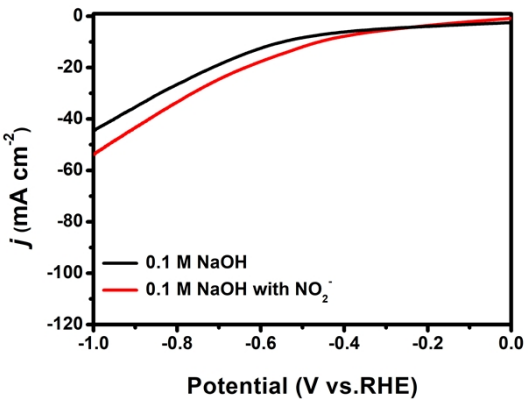

Fig. S9. LSV curves of JBC-800/CP in 0.1 M NaOH with and without NO_2^-.

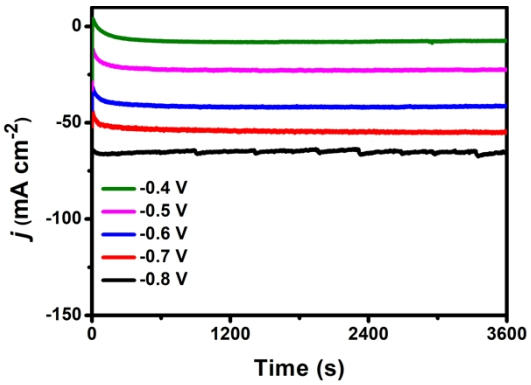

Fig. S10. Chronoamperometry curves at different potentials in 0.1 M NaOH with 0.1 M NO_2^-.

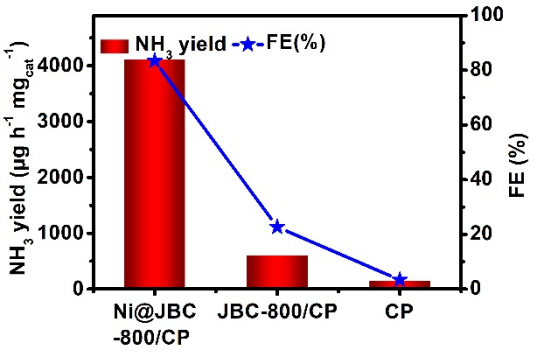

Fig. S11. Comparison of NH_3 yields and FEs for Ni@JBC-800/CP, JBC-800/CP and CP at –0.5 V.

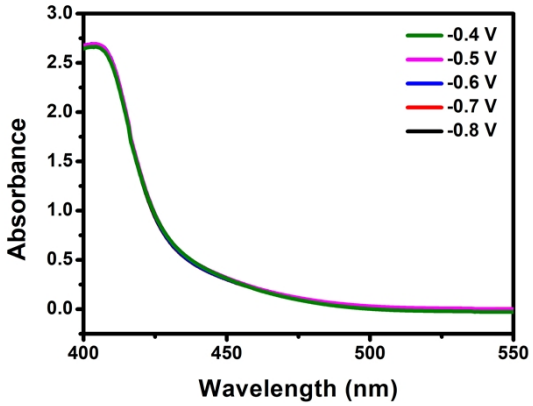

Fig. S12. UV-Vis spectra of electrogenerated N_2H_4 for Ni@JBC-800/CP at different given potentials.

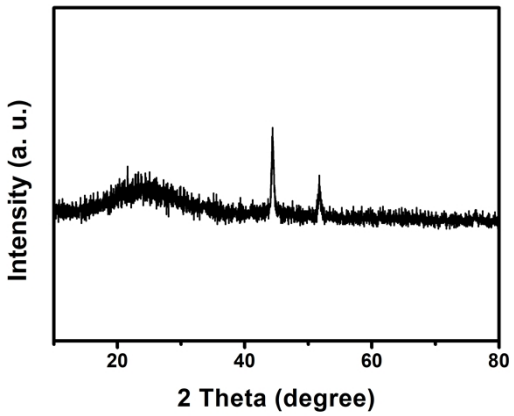

Fig. S13. XRD pattern of Ni@JBC-800 after12-h electrolysis.

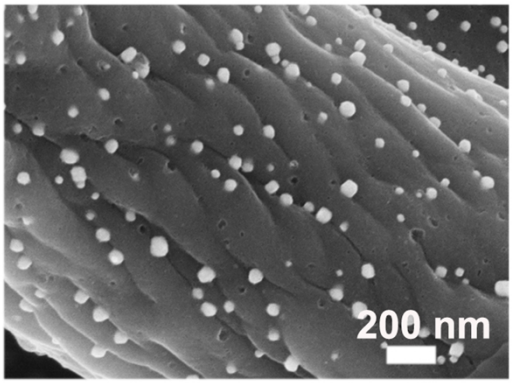

Fig. S14. SEM image of Ni@JBC-800 after 12-h electrolysis.

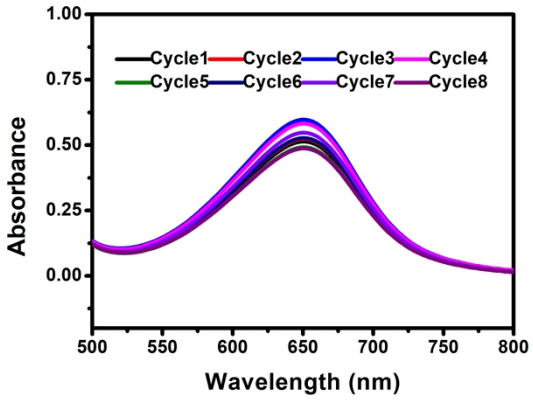

Fig. S15. UV-Vis spectra of Ni@JBC-800 for electrogenerated NH_3 during recycling tests at –0.5 V in 0.1 M NaOH with 0.1 M NO_2^-.

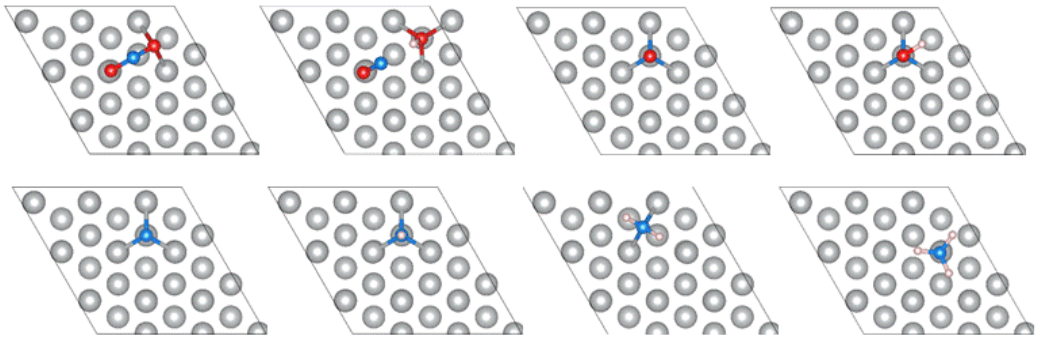

Fig. S16. Atomic configurations of the adsorbed intermediates for NO_2^-RR on Ni (111).

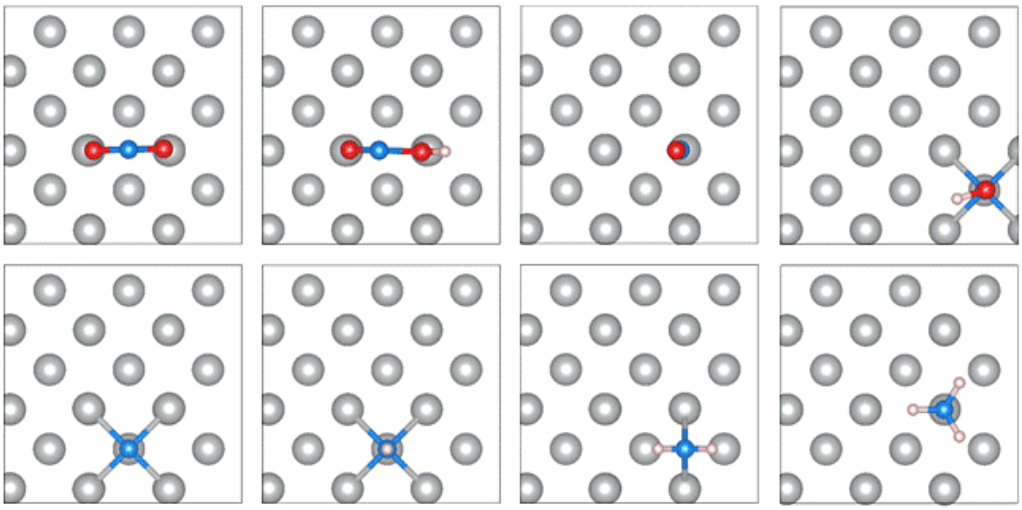

Fig. S17. Atomic configurations of the adsorbed intermediates for NO_2^-RR on Ni (200).

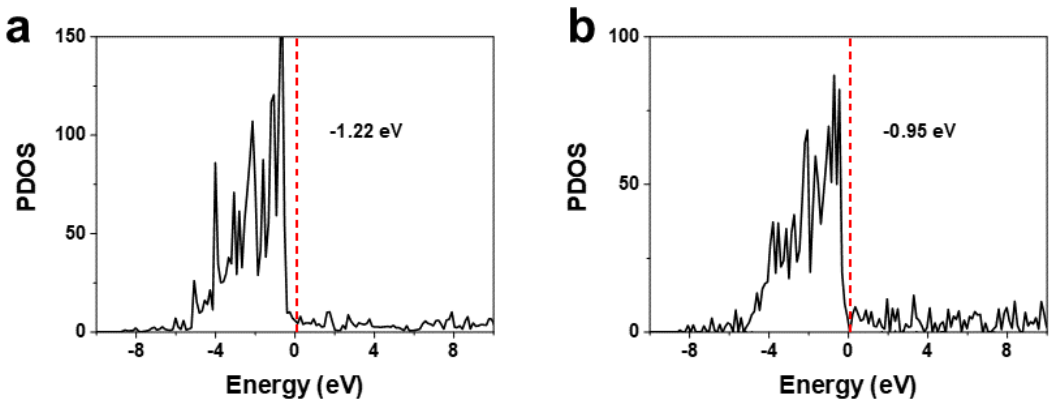

Fig. S18. PDOS of (a) Ni (111) and (b) Ni (200).

Table S1 Comparison of catalytic performances of Ni@JBC-800/CP with other reported non-noble-metal NO_2^-RR electrocatalysts.

Catalyst	Electrolyte	NH_3 yield	FE (%)	Ref.
Ni@JBC-800	0.1 M NaOH (0.1 M NO_2^-)	4117.3 μg h^{-1} $mg_{cat.}^{-1}$	83.4	This work
Ni-NSA-VNi	0.2 M Na_2SO_4 (200 ppm $NaNO_2$)	4011.66 μg h^{-1} cm^{-2}	88.9	10
MnO_2 nanoarrays	0.1 M Na_2SO_4 ($NaNO_2$)	1.89 μg $h^{-1}cm^{-2}$	6	11
Cobalt-tripeptide complex	1.0 M MOPS (1.0 M $NaNO_2$)	18.42 μg h^{-1} cm^{-2}	90 ± 3	12
CoP NA/TM	0.1 M PBS (500 ppm $NaNO_2$)	2260.7 ± 51.5 μg·h^{-1}·cm^{-2}	90.0 ± 2.3	13
Cu_3P nanoarray	0.1 M PBS (500 ppm $NaNO_2$)	1626.6 ± 36.1 μg h^{-1} cm^{-2}	91.2 ± 2.5	14
$Cu_{80}Ni_{20}$	1.0 M NaOH (20 mM $NaNO_2$)	–	87.6	15
Cu nanosheets	0.1 M KOH	390.1 μg h^{-1} mg^{-1}	99.7	16
Ni_2P nanosheet array	0.1 M PBS (200 ppm $NaNO_2$)	2692.2 ± 92.1 μg h^{-1} cm^{-2}	90.2 ± 3	17
CuPc	0.1 M KOH (0.1 M KNO_2)	–	78	18

References

1 G. Kresse and J. Furthmüller, *Phys. Rev. B*, 1996, **54**, 11169.

2 G. Kresse and J. Furthmüller, *J. Comp. Mater. Sci.*, 1996, **6**, 15–50.

3 G. Kresse and J. Hafner, *Phys. Rev. B*, 1994, **49**, 14251–14269.

4 M. D. Segall, P. J. D. Lindan, M. J. Probert, C. J. Pickard, P. J. Hasnip, S. J. Clark and M. C. Payne, *J. Phys. Condens. Matter*, 2002, **14**, 2717–2744.

5 P. E. Blöchl, *Phys. Rev. B*, 1994, **50**, 17953.

6 J. P. Perdew, J. A. Chevary, S. H. Vosko, K. A. Jackson, M. R. Pederson, D. J. Singh and C. Fiolhais, *Phys. Rev. B*, 1992, **46**, 6671.

7 S. Grimme, J. Antony, S. Ehrlich and H. A. Krieg, *J. Chem. Phys.*, 2010, **132**, 154104.

8 H. J. Monkhorst and J. D. Pack, *Phys. Rev. B*, 1976, **13**, 5188.

9 J. Norskov, J. Rossmeisl, A. Logadottir, L. Lindqvist, J. Kitchin, T. Bligaard, and H. Jonsson, *J. Phys. Chem. B*, 2004, **108**, 17886–17892.

10 C. Wang, W. Zhou, Z. Sun, Y. Wang, B. Zhang and Y. Yu, *J. Mater. Chem. A,* 2021, **9**, 239–243.

11 R. Wang, Z. Wang, X. Xiang, R. Zhang, X. Shi and X. Sun, *Chem. Commun.,* 2018, ***54***, 10340–10342.

12 Y. Guo, J. R. Stroka, B. Kandemir, C. E. Dickerson and K. L. Bren, *J. Am. Chem. Soc.*, 2018, **140**, 16888–16892.

13 G. Wen, J. Liang, Q. Liu, T. Li, X. An, F. Zhang, A. A. Alshehri, K. A. Alzahrani, Y. Luo, Q. Kong and X. Sun, *Nano Res.*, 2022, **15**, 972–977.

14 J. Liang, B. Deng, Q. Liu, G. Wen, Q. Liu, T. Li, Y. Luo, A. A. Alshehri, K. A. Alzahrani, D. Ma and X. Sun, *Green Chem*., 2021, **23**, 5487–5493.

15 L. Mattarozzi, S. Cattarin, N. Comisso, P. Guerriero, M. Musiani, L. Vázquez-Gómez and E. Verlato, *Electrochim. Acta*, 2013, **89**, 488–496.

16 X. Fu, X. Zhao, X. Hu, K. He, Y. Yu, T. Li, Q. Tu, X. Qian, Q. Yue, M. Wasielewski and Y. Kang, *Appl. Mater. Today*, 2020, **19**, 100620.

17 G. Wen, J. Liang, L. Zhang, T. Li, Q. Liu, X. An, X. Shi, Y. Liu, S. Gao, A. M. Asiri, Y. Luo, Q. Kong and X. Sun, *J. Colloid Interf. Sci.*, 2022, **606**, 1055–1063.

18 N. Chebotareva and T. Nyokong, *J. Appl. Electrochem.*, 1997, **27**, 975–981.